Lawrence Berkeley National Laboratory

Title

Tuning the interlayer coupling in La0.7Sr0.3Mn0.95Ru0.05O3/LaNiO3 multilayers with perpendicular magnetic anisotropy

Permalink

Journal

ISSN

Authors

Schöpf, Jörg

Piva, Valentina

van Loosdrecht, Paul HM

et al.

Publication Date

DOI

Copyright Information

Tuning the interlayer coupling in La$_{0.7}$Sr$_{0.3}$Mn$_{0.95}$Ru$_{0.05}$O$_3$/LaNiO$_3$ multilayers with perpendicular magnetic anisotropy

Jörg Schöpf [*], Valentina Piva, Paul H. M. van Loosdrecht, and Ionela Lindfors-Vrejoiu [†]

Institute of Physics II, University of Cologne, 50937 Cologne, Germany

Padraic Shafer

Advanced Light Source, Lawrence Berkeley National Laboratory, Berkeley, California 94720, USA

Divine P. Kumah and Xuanyi Zhang

Department of Physics, Duke University, Durham, North Carolina 27517, USA
and Department of Physics, North Carolina State University, Raleigh, North Carolina 27695, USA

Lide Yao

OtaNano-Nanomicroscopy Center, Aalto University, P.O. Box 15100, FI-00076 Aalto, Finland

Sebastiaan van Dijken

Department of Applied Physics, Aalto University School of Science, P.O. Box 15100, FI-00076 Aalto, Finland

In ferromagnetic oxide epitaxial multilayers, magnetic properties and interlayer coupling are determined by a variety of factors. Beyond the contribution of interlayer exchange coupling, strain and interfacial effects, such as structural reconstructions or charge transfer, play significant roles, resulting in complex magnetic behavior. In this study, the interlayer coupling of ferromagnetic La$_{0.7}$Sr$_{0.3}$Mn$_{0.95}$Ru$_{0.05}$O$_3$ (LSMRO) layers (8 nm thick) was investigated, when separated by epitaxial spacers of paramagnetic metallic LaNiO$_3$ (LNO), in stacks exhibiting perpendicular magnetic anisotropy. By varying the thickness of the spacer, it was found that the coupling between two LSMRO layers changes from antiferromagnetic (with a 4-unit-cell-thick LNO spacer) to ferromagnetic (with a 6-unit-cell-thick LNO spacer). For multilayers comprising five LSMRO layers and a 4-unit-cell-thick LNO spacer, the antiferromagnetic coupling was preserved. However, the effective magnetic anisotropy changed, causing the magnetization to cant more towards the in-plane direction. This behavior was corroborated by X-ray magnetic circular dichroism (XMCD) investigations at the Mn and Ni L_3 edges. The XMCD results indicated that the 4-unit-cell-thick LNO spacer in the multilayer become magnetically ordered, closely following the magnetization of adjacent LSMRO layers.

I. INTRODUCTION

Ferromagnetic oxides, especially the perovskite mixed-valence manganites with ordering temperatures exceeding room temperature, are a propitious material class for epitaxial heterostructures research [1,2]. Perovskite manganites exhibit a delicate balance among competing interactions involving lattice, electronic, and spin degrees of freedom [3]. Recent studies have revealed complex noncollinear magnetic order in La$_{0.67}$Sr$_{0.33}$MnO$_3$-LaNiO$_3$ superlattices with in-plane magnetic anisotropy [4,5], as well as magnetic skyrmion bubbles in La$_{0.7}$Sr$_{0.3}$Mn$_{1-x}$Ru$_x$O$_3$ multilayers with perpendicular magnetic anisotropy [6].

In magnetic multilayers, the type and the strength of interlayer coupling [7,8] are crucial for determining their properties and realizing unique effects that are useful for applications, such as giant magnetoresistance (GMR) [9]. For magnetic oxide epitaxial multilayers, the exploration of metallic nonmagnetic oxides as spacer layers, enabling control over the type of coupling and compatible with coherent growth, has been less extensive compared to simpler ferromagnetic multilayers developed during the discovery of GMR. In comparison to the simple metallic ferromagnetic multilayers, such as Fe/Cr or Co/Pt, magnetic oxide multilayers offer many possibilities to tailor their magnetic properties, for example by the strain imposed by the epitaxial growth. Moreover, their crystalline and interface quality exceeds that of the typically polycrystalline metallic multilayers. Additionally, mixed-valence manganites have exciting magnetotransport properties, supplemented by their propensity toward electric-field-effect manipulation in gating devices. Concerning the interlayer coupling, recent findings demonstrated that for SrRuO$_3$ epitaxial layers with perpendicular magnetic anisotropy (PMA), the interlayer coupling is strongly ferromagnetic with

---

[*]Contact author: schoepf@ph2.uni-koeln.de
[†]Contact author: vrejoiu@ph2.uni-koeln.de

4-unit-cell-thick LaNiO$_3$ spacers [10], whereas SrIrO$_3$ spacer layers keep the SrRuO$_3$ decoupled [11]. In the work on SrRuO$_3$/LaNiO$_3$ multilayers, the aim was to obtain strongly ferromagnetic coupling between SrRuO$_3$ layers, and no antiferromagnetic coupling was reported [10]. However, the use of paramagnetic metallic LaNiO$_3$ (LNO) spacer layers has been reported to result in oscillatory exchange coupling via the Ruderman-Kittel-Kasuya-Yosida (*RKKY*) interaction in La$_{0.67}$Ba$_{0.33}$MnO$_3$/LNO heterostructures with in-plane magnetic anisotropy [12,13]. However, given the low thickness of the LNO spacers used in these multilayers, the additional role of tunneling cannot be entirely ruled out.

In this work, we investigated the interlayer coupling between La$_{0.7}$Sr$_{0.3}$Mn$_{0.95}$Ru$_{0.05}$O$_3$ (LSMRO) ferromagnetic layers with PMA, mediated by a LNO spacer layer. The PMA of the LSMRO layers arises from the modification of anisotropy due to Ru substitution of Mn, and the compressive strain from epitaxial growth on (LaAlO$_3$)$_{0.3}$-(Sr$_2$TaAlO$_6$)$_{0.7}$ (LSAT) substrates [14–17]. We demonstrated that LNO is a suitable spacer material for LSMRO layers, enabling the tailoring of the interlayer coupling from antiferromagnetic (AFM) to ferromagnetic (FM) by adjusting the LNO thickness, likely through an *RKKY*-type of mechanism [12,13]. Controlling the coupling type between LSMRO layers enables the design of multilayers in which magnetic domains can couple either ferromagnetically or antiferromagnetically. Antiferromagnetic coupling in ferromagnetic oxide heterostructures is less commonly reported, although it holds significant promise, especially in the emerging field of antiferromagnetic spintronics [18] and memory devices [19]. Synthetic antiferromagnets, consisting of two or more magnetic layers separated by spacers and coupled antiferromagnetically, are envisioned for the development of faster, smaller, more energy-efficient, and robust heterostructures that can enhance the information encoding in ultrahigh density spin-transfer-torque magnetic random access memory cells [20]. Furthermore, skyrmion bubbles in synthetic antiferromagnetic multilayers benefit from reduced skyrmion Hall-effect perturbations in their current-induced motion [21]. As the generation and density of skyrmions are strongly dependent on interlayer exchange coupling and easy-axis orientation [22], understanding the strength of the coupling and how it changes with modifications in effective magnetic anisotropy in multilayers is of paramount importance.

II. SAMPLE DESIGN AND METHODS

The samples were fabricated by using pulsed-laser deposition (PLD), assisted by reflection high-energy electron diffraction (RHEED), as described in detail in previous publications [6,16]. Trilayer samples with two LSMRO layers (about 8 nm thick) separated by a LNO spacer of either 4 unit cells (uc) or 6 uc thickness, as shown in Fig. 1(a), and multilayers with five LSMRO layers (about 8 nm thick) separated by four LNO spacers, were grown on LSAT(100) substrates (these substrates were square shaped, measuring either 4 or 5 mm). Prior to PLD, the LSAT substrates were annealed at 1000 °C in air for 2 h.

A homemade setup was used for simultaneous polar magneto-optic Kerr effect (MOKE) and magnetotransport
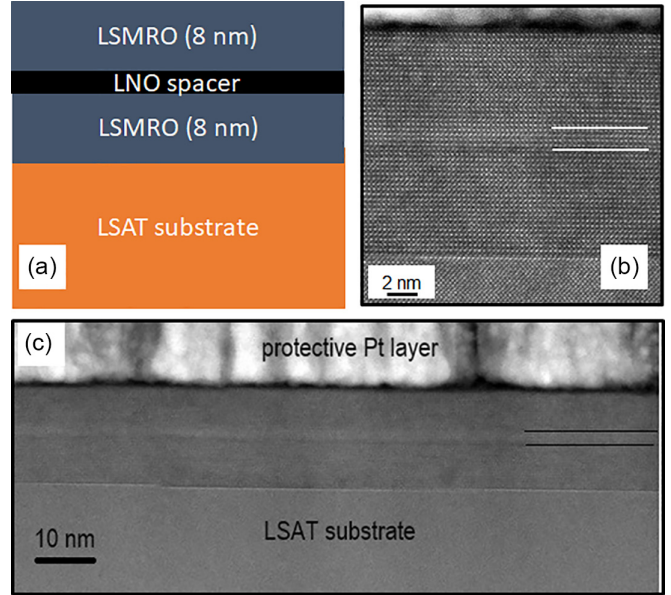

FIG. 1. Structure of the samples used for the investigation of interlayer coupling. (a) Schematic drawing of the trilayer samples. (b) High magnification HAADF-STEM image of the cross-section of a trilayer sample with a 4-uc-thick LNO spacer, marked by the white horizontal lines. (c) Low magnification overview HAADF-STEM image of the same sample, with the two black lines delineating the LNO spacer (the Pt protective layer was deposited for STEM specimen preparation).

measurements. MOKE measurements utilized a double modulation technique with an optical chopper and a photoelastic modulator (PEM100, Hinds Instruments). Light sources included a Xe lamp with a Jobin Yvon monochromator and a 405 nm Cobolt laser. Magnetotransport measurements were performed using the van der Pauw geometry, with electrical contacts made by gluing copper wires to the sample corners using silver paint. SQUID magnetometry was carried out with a commercially available SQUID magnetometer (MPMS-XL, Quantum Design, Inc.). Scanning transmission electron microscopy (STEM) of cross-section specimens was conducted with a JEOL 2200FS TEM, equipped with double C$_s$ (spherical aberration) correctors and operated at 200 keV. STEM specimens were prepared by focused ion beam (JEOL JIB-4700F) milling with a Ga ion source. A 1.5 µm Pt layer was deposited on the surface prior to milling to mitigate ion beam damage.

X-ray absorption spectroscopy (XAS) and X-ray magnetic circular dichroism (XMCD) measurements were performed at the 4.0.2 beamline at the Advanced Light Source. Absorption spectra were recorded at the Mn-*L* and Ni-*L* edges using total electron yield (TEY) and luminescence yield (LY) detection modes, at 80 K. LY measurements were particularly effective for probing the buried LNO layers compared to the surface-sensitive TEY measurements.

III. RESULTS AND DISCUSSION

The microstructure of the epitaxial heterostructures was investigated by RHEED during growth, which also enabled
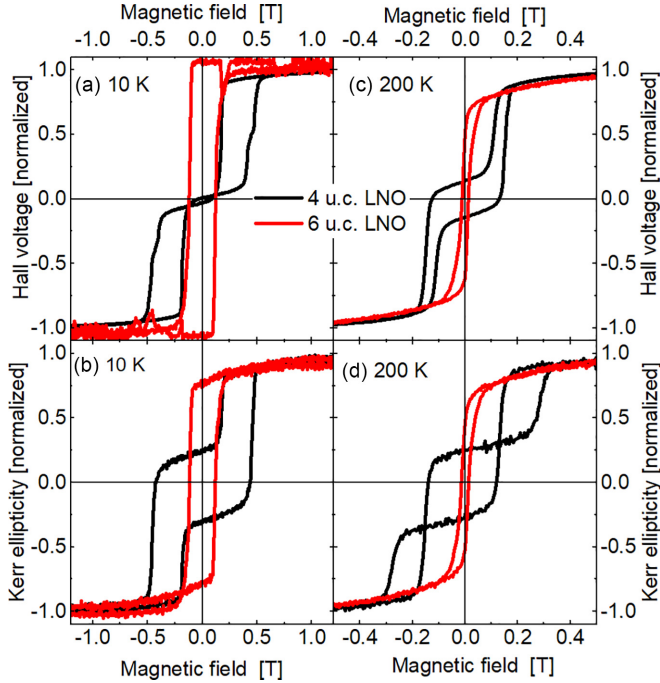
FIG. 2. Hysteresis loops of the trilayer samples: (a) Normalized (anomalous) Hall voltage loops, respectively, of samples with a 4-uc-thick LNO spacer (black) and a 6-uc-thick LNO spacer (red) at 10 K. (b) Kerr ellipticity loops of the same trilayer at 10 K. (c) and (d) The same measurements as in (a) and (b), recorded at 200 K. The magnetic field was applied perpendicular to the sample surface.

accurate control over the layer thickness, and postgrowth analysis was conducted via atomic force microscopy and STEM. High-angle annular dark field (HAADF)-STEM micrographs of a cross-section specimen of a trilayer sample with a 4-uc-thick LNO spacer are shown in Figs. 1(b) and 1(c). The spacer layer is continuous, with no pinholes or significant deviations from the nominal 4 uc thickness. Additional microstructural investigations are provided in the supplemental material [23].

To assess the type of coupling between LSMRO layers in the trilayer samples, full MOKE (ellipticity and Kerr rotation) and Hall effect measurements were performed simultaneously at temperatures ranging from 10 to 200 K in a perpendicular magnetic field, as the LSMRO layers exhibit PMA. Data demonstrating the PMA of reference samples, including a single 8-nm-thick LSMRO layer and a bilayer with 6 uc LNO on an 8-nm-thick LSMRO layer, are discussed in the supplemental material [23]. Figure 2 summarizes the normalized Hall voltage and Kerr ellipticity loops of the two type of trilayers, with 4 and 6 uc LNO spacers, measured at 10 and 200 K. These spacer thicknesses were chosen based on the expectation that 4 uc LNO would result in AFM coupling and 6 uc LNO would result in FM coupling, similar to $La_{0.67}Ba_{0.33}MnO_3$-$LaNiO_3$ heterstructures with in-plane anisotropy [12]. For the Hall voltage loops, the normal Hall effect contribution was subtracted, leaving only the anomalous Hall effect, which is proportional to the perpendicular magnetization of the sample. No topological Hall effect contribution was expected to the Hall effect measurements of these heterostructures, because no conditions for the

formation of skyrmions were met by any of the heterostructures. For the 6 uc LNO spacer, a single loop with a sharp magnetization reversal (red loops) is observed, indicating FM coupling and simultaneous magnetization reversal in the two LSMRO layers. In contrast, the trilayer with a 4 uc LNO spacer shows hysteresis loops (black loops in Fig. 2) characteristic of AFM-coupled layers [19,24]: a sharp step occurs at positive fields of about 0.2 T at 10 K and at 0.13 T at 200 K when decreasing the field from positive saturation to zero. The AFM exchange field is about 0.35 T at 10 K and 0.15 T at 200 K. Despite the expectation that for a perfectly antiferromagnetic coupling of two identical ferromagnetic layers the remnant magnetization of the heterostructures should be zero, both the MOKE and Hall loops from Fig. 2 show some finite remnance. In these heterostructures, although the two LSMRO layers were meant to be nominally identical, their strain state and microstructure are influenced by their position in the stack, and thus the magnetic properties of the two layers are slightly different. Moreover, the MOKE loops are strongly influenced by optical interference effects, such as those reported in [16]. The Hall voltage loops of the heterostructures, measured in van der Pauw geometry, are also the complex result of the partition of the excitation current through the two LSMRO layers and the LNO conductive spacer. In other oxide systems, AFM interlayer coupling has been achieved between two $La_{0.67}Ca_{0.33}MnO_3$ layers with in-plane magnetic anisotropy separated by insulating $CaRu_{0.5}Ti_{0.5}O_3$ [25]. However, for this multilayer, the insulating nature of the spacer material suggests that tunneling, rather than *RKKY*, likely dominates the interlayer coupling. The magnetization loops of the samples studied by Jin *et al.* exhibited similar behavior as the Hall and MOKE loops of our trilayer samples, as summarized in Fig. 2. The AFM exchange field for the $La_{0.67}Ca_{0.33}MnO_3$/$CaRu_{0.5}Ti_{0.5}O_3$ heterostructures in this study was about 30 mT at 20 K.

Multilayers with five LSMRO layers and 4-uc-thick LNO spacers, made under the same conditions, were studied as well. For an odd number of LSMRO layers, it is expected that a finite net magnetization exists at remanence even for AFM interlayer coupling [24]. The microstructure of the multilayer was investigated by STEM and energy-dispersive X-ray spectroscopy (EDX), with a summary shown in Fig. 3. The layers, particularly the ultrathin LNO layers, exhibit uniform thickness and sharp interfaces. EDX elemental maps confirm that the Ni signal is confined within the 4-uc-thick spacers.

SQUID magnetometry measurements of a multilayer revealed that the effective magnetic anisotropy changes relative to the trilayer samples, and that the LNO layers contribute to the magnetization. Figure 4(a) summarizes the magnetometry measurements. Magnetic hysteresis loops for a perpendicular field as a function of temperature are plotted in Fig. 4(a). All loops are corrected by subtracting the contribution of the LSAT substrate, which is diamagnetic and has a significant paramagnetic signal at low temperatures (see the supplemental material) [23]. The magnetization loop shapes indicate that AFM-coupling exists between the LSMRO layers, as magnetization reversal starts at positive fields when the field is reduced from positive saturation. A minor loop starting from saturation in high positive field and reversing at 0.2 T shows a shift in the positive direction, consistent with AFM coupling (see
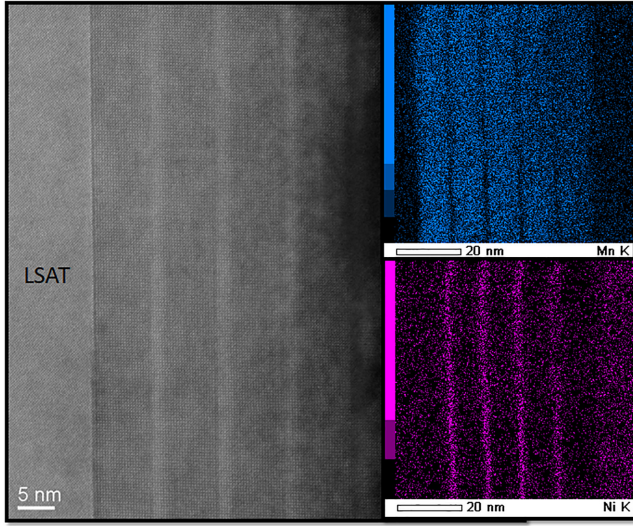
FIG. 3. High magnification HAADF-STEM image of the cross section of a multilayer with 4-uc-thick LNO spacers between five 8-nm-thick LSMRO layers. The images on the right are EDX elemental maps, showing the distribution of Mn (top; blue) and Ni (bottom; magenta).
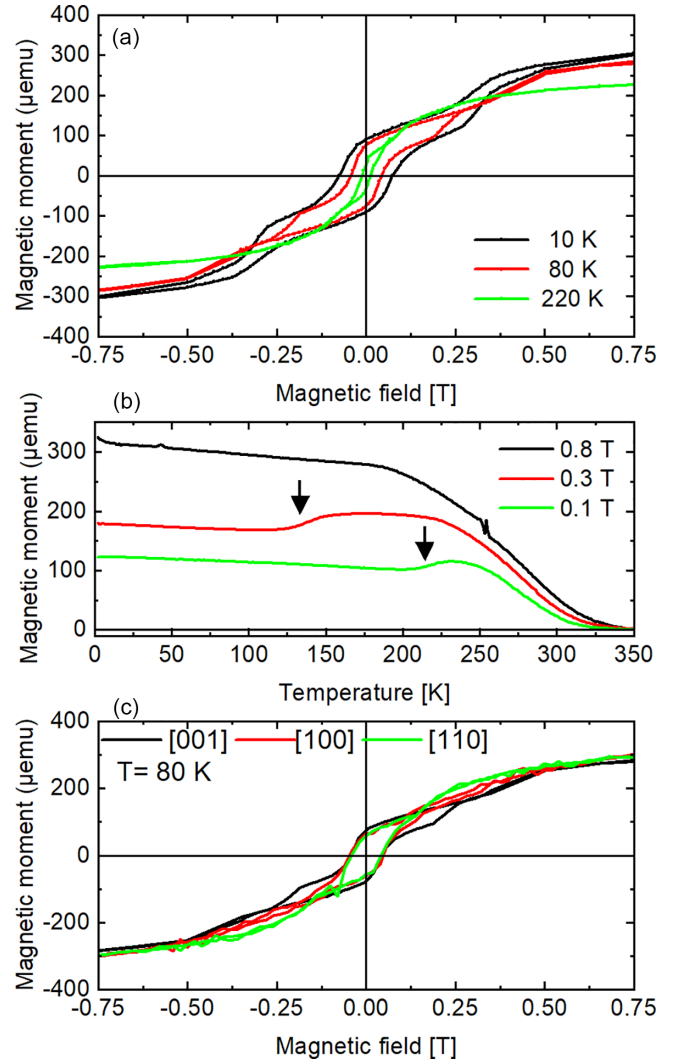

FIG. 4. SQUID magnetometry measurements of a multilayer with five LSMRO layers and 4-uc-thick LNO spacers. (a) Full loops of the magnetization reversal as a function of applied field at 10, 80, and 220 K, with the field perpendicular to the sample. (b) Magnetization as a function of temperature measured by field cooling, for different values of magnetic field along the direction perpendicular to the sample. The black arrows mark the anomalous behavior arising from the AFM-coupling between the LSMRO layers. (c) Magnetization loops for the field applied along different cubic axes, with [001] perpendicular to the sample, at 80 K.

supplemental material). The presence of AFM-coupling is further supported by the behavior of the magnetization curves measured under field-cooling conditions: for lower applied fields (0.1 to 0.3 T, similar to the AFM exchange field), the curves exhibit an anomalous dip, with its position depending on field value [see Fig. 4(b), where the dip is marked by black arrows]. The dip is suppressed in the $M(T)$ curve measured at 0.8 T, as this field value exceeds the AFM exchange field values at all temperatures down to 10 K. Similar $M(T)$ behavior has been observed for antiferromagnetically coupled $La_{0.67}Ca_{0.33}MnO_3/CaRu_{1/2}Ti_{1/2}O_3$ multilayers [26]. The mechanism of layer-resolved magnetization reversal discussed in Refs. [24,26] is plausible for the LSMRO/LNO multilayers as well. However, the loops for the multilayer with five LSMRO layers appear to exhibit only three reversal steps. The magnetization reversal is more complex for the perpendicularly magnetized multilayers than for those with in-plane anisotropy, such as those discussed in Ref. [26]. Picturing how the magnetization reversal occurs from measurements of $M(H)$ loops alone, without the magnetic domain formation imaging, is thus only tentative. The hysteresis loop shape is strongly influenced by the measurement conditions (i.e., field sweep rate) and by magnetic domain formation, such as stripe domains with alternating up-down perpendicular magnetization, due to the strong demagnetization effects present in the PMA conditions. It can be tentatively proposed that the magnetization reverses similarly to the mechanism described in Ref. [27] for $La_{0.7}Sr_{0.3}MnO_3/SrRuO_3$ superlattices at 100 K. In Ref. [27], it was found that for in-plane magnetic fields, the magnetically harder $SrRuO_3$ layers reverse their magnetization first in positive fields and align antiparallel to the magnetization of the magnetically softer $La_{0.7}Sr_{0.3}MnO_3$ layers, resulting in a ferrimagnetic-like superstructure. Reducing the magnetic field to zero and reversing its polarity, this ferrimagnetic-like coupled superstructure switches its overall

magnetization 180°, following the applied field. In higher negative magnetic fields, the $SrRuO_3$ layers of the superlattice also turn the magnetization parallel to the in-plane applied field, and the magnetization of the superlattice reaches saturation eventually. However, it cannot be discriminated solely from the behavior of the $M(H)$ loops how the uncompensated antiferromagnetic synthetic structure reverses its magnetization. The reversal could take place via the formation of a vertically and a horizontally heterogeneous state of mixed FM/AFM stripe domains or via a continuous spin-flop type of transition, in which the magnetization of each of the five layers is significantly canted (as described in Fig. 1 of [28]). These two scenarios proposed for the collective magnetization

reversal explain better the magnitude of the ratio between the remnant magnetization and the saturation magnetization of the M(H) loops measured by SQUID magnetometry. The competition between the effective uniaxial magnetic anisotropy of the multilayer and the strength of the antiferromagnetic exchange coupling dictates which of the scenarios is physically more realistic. The effective magnetic anisotropy of the multilayer changed significantly compared to the single LSMRO layer and trilayer samples, which have strong PMA. Figure 4(c) shows the magnetization loops as a function of field direction measured at 80 K. Loops were measured with perpendicular field (along the [001] direction) and with in-plane field along the sample edge ([100] direction) or parallel to the sample diagonal ([110] direction). The comparison of the loops indicates that the effective magnetic anisotropy is no longer dominantly perpendicular to the multilayer surface, as the three loops have similar coercive fields and saturation magnetization, and only slightly different saturation fields. Field-cooling M(T) curves measured in three different field directions confirm this statement (data shown in the supplemental material) [23]. This apparent change in effective magnetic anisotropy, impacting the squareness of the magnetization loops, is partly due to the increased stack thickness (relative to trilayer samples), resulting in a larger contribution of dipolar interactions. The dipolar interactions favor FM coupling between layers and the formation of magnetic stripe domains and/or in-plane reorientation of the magnetization and spin-flop transitions [24,28,29].

XMCD measurements at the Mn L-edge and the Ni L-edge were performed in LY-detection mode to probe the buried LNO layers better [30]. XMCD is determined from the difference in XAS measurements for right and left circularly polarized incident light. Figure 5 shows hysteresis loops measured for the Mn L-edge and Ni L-edge, for perpendicular and in-plane fields, at 80 K. The in-plane Mn signal is significantly stronger, indicating in-plane canting of the magnetization of the LSMRO layers, in qualitative agreement with the SQUID magnetometry data. However, the SQUID loops for in-plane and out-of-plane geometries showed similar magnitudes of the magnetic moment [see Fig. 4(c)]. Differences between the SQUID magnetometry, which measures the whole sample, and XMCD experiments, which are mainly sensitive to the topmost layers of the sample, can explain discrepancies between the two types of loops. Nonetheless, the shape of the XMCD Mn loops resembles well that of SQUID loops. Additional differences may arise from contributions in the magnetometry loops from the LSAT substrate and from the four LNO layers. For a comparison of SQUID and XMCD normalized loops, see the supplemental material [23]. Both the perpendicular and in-plane field Mn loops show a sharp initial drop where AFM coupling induces the first switching of two layers (marked by the vertical lines in Fig. 5), followed by an almost linear decrease as the field is reduced to zero and changes its polarity. AFM coupling is overcome in higher fields, leading to a sharp step after which the magnetization again reaches saturation. The linear part strongly indicates the presence of laterally growing stripe domains in the LSMRO layers, indicating that the scenario of mixed FM/AFM stripe domains proposed in Fig. 1 of [28] may be more relevant for our multilayers. Stripe domains forming in perpendicular
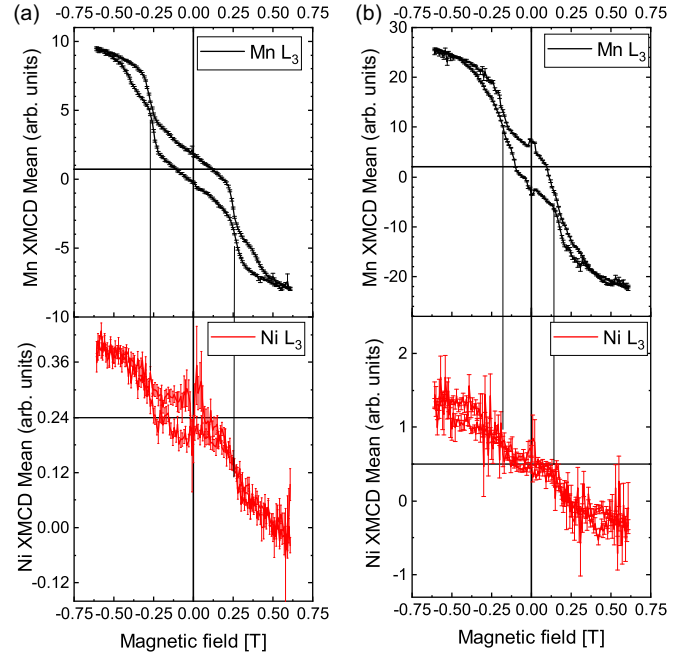

FIG. 5. XMCD investigations of a multilayer with five LSMRO layers and 4-uc-thick LNO spacers (at 80 K). Loops for Mn L-edge (black, top) and for Ni L-edge (red, bottom), measured (a) with perpendicular magnetic field and (b) with in-plane magnetic field, in LY conditions.

fields have been observed in 30–40-nm-thick LSMRO films grown on LSAT substrates [14,17]. The magnetic domains in our AFM-coupled LSMRO multilayers are likely more complex, as they may be mixed FM/AFM stripes [28,29,31], and require further imaging investigations in perpendicular fields, such as cryogenic magnetic force microscopy.

Regarding the LNO spacer layers, there is a sizable but weak XMCD Ni-signal indicating magnetic ordering in the LNO layers. The Ni loops suggest that the magnetization of the LNO layers is coupled and follows the magnetization reversal of the LSMRO layers. In $La_{2/3}Ca_{1/3}MnO_3/LaNiO_3$ superlattices grown on $SrTiO_3$ substrates with in-plane magnetic anisotropy, emerging magnetism in LNO was inferred through an exchange bias mechanism at the interfaces observed by X-ray resonant magnetic reflectivity. Soltan *et al.* found nonsymmetric interfaces induced magnetization profiles in LNO and LCMO, related to a periodic complex charge and spin superstructure [32]. XMCD investigations of $LaMnO_3/LaNiO_3$ superlattices with ultrathin layers (4–7-uc-thick individual layers) and in-plane magnetic anisotropy also showed magnetic ordering of the nickelate layers, with Ni magnetic moments being ferromagnetically coupled to Mn magnetic moments [33].

IV. SUMMARY

Here, the interlayer coupling between epitaxial $La_{0.7}Sr_{0.3}Mn_{0.95}Ru_{0.05}O_3$ layers with perpendicular magnetic anisotropy, separated by nominally metallic paramagnetic $LaNiO_3$ ultrathin layers, was investigated. Using MOKE, anomalous Hall effect investigations, and

SQUID magnetometry, it was found that $LaNiO_3$ serves as a suitable spacer for tuning the interlayer coupling from antiferromagnetic to ferromagnetic by varying the spacer thickness. The coupling mechanism is of the *RKKY*-type, as discussed by prior studies [12,13]. Furthermore, multilayers with five $La_{0.7}Sr_{0.3}Mn_{0.95}Ru_{0.05}O_3$ layers separated by 4-uc-thick $LaNiO_3$ spacers were fabricated, showing that the antiferromagnetic interlayer coupling persisted. The magnetization reversal mechanism in the five $La_{0.7}Sr_{0.3}Mn_{0.95}Ru_{0.05}O_3$ layers between opposite saturated polarities was proposed, with observations indicating that the effective magnetic anisotropy in the multilayer canted more strongly towards to the in-plane direction, likely due to increased interactions. XMCD investigations revealed that the 4-uc-thick $LaNiO_3$ layers in the multilayer were magnetically ordered at 80 K, and their magnetization reversal followed that of the $La_{0.7}Sr_{0.3}Mn_{0.95}Ru_{0.05}O_3$ layers. This demonstrates control over the interlayer coupling between manganite layers with perpendicular magnetic anisotropy, achieving strong antiferromagnetic coupling relevant for spintronic applications, such as spin-valve devices. Future work will focus on LSMRO/LNO multilayers, exploring the dependence on thickness and the number of LSMRO layers, on the Ru content of the LSMRO layers, as well as the study of magnetic domains in antiferromagnetically coupled multilayers. These findings open up prospects for designing synthetically antiferromagnetic skyrmion bubbles in ferromagnetic oxide epitaxial multilayers, presenting exciting opportunities for advanced spintronic applications.

The supporting data for this article are available from Zenodo [34].

[1] Y. Ijiri, Coupling and interface effects in magnetic oxide superlattices, J. Phys.: Condens. Matter **14**, R947 (2002).

[2] A. Bhattacharya and S. J. May, Magnetic oxide heterostructures, Annu. Rev. Mater. Res. **44**, 65 (2014).

[3] K. Dörr, Ferromagnetic manganites: Spin-polarized conduction versus competing interactions, J. Phys. D **39**, R125 (2006).

[4] J. D. Hoffman, B. J. Kirby, J. Kwon, G. Fabbris, D. Meyers, J. W. Freeland, I. Martin, O. G. Heinonen, P. Steadman, H. Zhou, C. M. Schlepütz, M. P. M. Dean, S. G. E. te Velthuis, J.-M. Zuo, and A. Bhattacharya, Oscillatory noncollinear magnetism induced by interfacial charge transfer in superlattices composed of metallic oxides, Phys. Rev. X **6**, 041038 (2016).

[5] G. Fabbris, N. Jaouen, D. Meyers, J. Feng, J. D. Hoffman, R. Sutarto, S. G. Chiuzbäian, A. Bhattacharya, and M. P. M. Dean, Emergent *c*-axis magnetic helix in manganite-nickelate superlattices, Phys. Rev. B **98**, 180401(R) (2018).

[6] J. Schöpf, A. Thampi, P. Milde, D. Ivaneyko, S. Kondovych, D. Y. Kononenko, L. M. Eng, L. Jin, L. Yang, L. Wysocki, P. H. M. van Loosdrecht, K. Richter, K. V. Yershov, D. Wolf, A. Lubk, and I. Lindfors-Vrejoiu, Néel skyrmion bubbles in $La_{0.7}Sr_{0.3}Mn_{1-x}Ru_xO_3$ multilayers, Nano Lett. **23**, 3532 (2023).

[7] M. D. Stiles, Exchange coupling in magnetic heterostructures, Phys. Rev. B **48**, 7238 (1993).

[8] M. Stiles, Interlayer exchange coupling, J. Magn. Magn. Mater. **200**, 322 (1999).

[9] M. N. Baibich, J. M. Broto, A. Fert, F. Nguyen Van Dau, F. Petroff, P. Etienne, G. Creuzet, A. Friederich, and J. Chazelas, Giant magnetoresistance of (001)Fe/(001)Cr magnetic superlattices, Phys. Rev. Lett. **61**, 2472 (1988).

[10] L. Yang, L. Jin, L. Wysocki, J. Schöpf, D. Jansen, B. Das, L. Kornblum, P. H. M. van Loosdrecht, and I. Lindfors-Vrejoiu, Enhancing the ferromagnetic interlayer coupling between epitaxial srruo3 layers, Phys. Rev. B **104**, 064444 (2021).

[11] L. Wysocki, S. E. Ilse, L. Yang, E. Goering, F. Gunkel, R. Dittmann, P. H. M. van Loosdrecht, and I. Lindfors-Vrejoiu, Magnetic interlayer coupling between ferromagnetic $SrRuO_3$ layers through a $SrIrO_3$ spacer, J. Appl. Phys. **131**, 133902 (2022).

[12] K. R. Nikolaev, A. Y. Dobin, I. N. Krivorotov, W. K. Cooley, A. Bhattacharya, A. L. Kobrinskii, L. I. Glazman, R. M. Wentzovitch, E. D. Dahlberg, and A. M. Goldman, Oscillatory exchange coupling and positive magnetoresistance in epitaxial oxide heterostructures, Phys. Rev. Lett. **85**, 3728 (2000).

[13] T. Ohsawa, S. Kubota, H. Itoh, and J. Inoue, Interlayer exchange coupling in perovskite-type magnetic trilayers, Phys. Rev. B **71**, 212407 (2005).

[14] M. Nakamura, D. Morikawa, X. Yu, F. Kagawa, T. Arima, Y. Tokura, and M. Kawasaki, Emergence of topological hall effect in half-metallic manganite thin films by tuning perpendicular magnetic anisotropy, J. Phys. Soc. Jpn. **87**, 074704 (2018).

[15] E. Hua, L. Si, K. Dai, Q. Wang, H. Ye, K. Liu, J. Zhang, J. Lu, K. Chen, F. Jin, L. Wang, and W. Wu, Ru-Doping-Induced Spin Frustration and Enhancement of the Room-Temperature Anomalous Hall Effect in $La_{2/3}Sr_{2/3}MnO_3$ Films, Adv. Mater. **34**, 2206685 (2022).

[16] J. Schöpf, P. H. M. van Loosdrecht, and I. Lindfors-Vrejoiu, Disentangling the magneto-optic Kerr effect of manganite epitaxial heterostructures, AIP Adv. **13**, 035319 (2023).

[17] L. Wysocki, Tunable magnetic anisotropy and magnetotransport properties of epitaxial oxide ferromagnetic heterostructures, Ph.D. thesis, University of Cologne, Germany, 2022.

[18] T. Jungwirth, X. Marti, P. Wadley, and J. Wunderlich, Antiferromagnetic spintronics, Nat. Nanotechnol. **11**, 231 (2016).

[19] Y. Saito, N. Tezuka, S. Ikeda, and T. Endoh, Antiferromagnetic interlayer exchange coupling and large spin Hall effect in

multilayer systems with Pt/Ir/Pt and Pt/Ir layers, Phys. Rev. B **104**, 064439 (2021).

[20] K. Wang, V. Bheemarasetty, and G. Xiao, Spin textures in synthetic antiferromagnets: Challenges, opportunities, and future directions, APL Mater. **11**, 070902 (2023).

[21] T. Dohi, S. DuttaGupta, S. Fukami, and H. Ohno, Formation and current-induced motion of synthetic antiferromagnetic skyrmion bubbles, Nat. Commun. **10**, 5153 (2019).

[22] J. Zhang, Y. Zhang, Y. Gao, G. Zhao, L. Qiu, K. Wang, P. Dou, W. Peng, Y. Zhuang, Y. Wu, G. Yu, Z. Zhu, Y. Zhao, Y. Guo, T. Zhu, J. Cai, B. Shen, and S. Wang, Magnetic skyrmions in a hall balance with interfacial canted magnetizations, Adv. Mater. **32**, 1907452 (2020).

[23] See Supplemental Material at http://link.aps.org/supplemental/10.1103/PhysRevMaterials.8.094410 for more details of the sample growth and structural characterization; for the magnetometry data of reference samples (single LSMRO layers); for analyses of the background corrections of the SQUID loops; minor loops; for a comparison of the XMCD and SQUID loops of the multilayer; and for AFM coupling investigation by field-cooled magnetization measurements for three different applied field directions.

[24] E. Darwin, R. Tomasello, P. M. Shepley, N. Satchell, M. Carpentieri, G. Finocchio, and B. J. Hickey, Antiferromagnetic interlayer exchange coupled $Co_{68}B_{32}$/Ir/Pt multilayers, Sci. Rep. **14**, 95 (2024).

[25] F. Jin, J. Shao, Z. Zhang, W. Zhang, K. Liu, J. Li, K. Liu, K. Dai, Q. Wang, Q. Lv, E. Hua, P. Chen, Z. Huang, C. Ma, L. Wang, Y. Zhao, and W. Wu, Measurement geometry and hydrostatic pressure-dependent magnetoresistance in all-oxide-based synthetic antiferromagnets, Adv. Funct. Mater. **33**, 2303492 (2023).

[26] B. Chen, H. Xu, C. Ma, S. Mattauch, D. Lan, F. Jin, Z. Guo, S. Wan, P. Chen, G. Gao, F. Chen, Y. Su, and W. Wu,

All-oxide-based synthetic antiferromagnets exhibiting layer-resolved magnetization reversal, Science **357**, 191 (2017).

[27] M. Ziese, I. Vrejoiu, and D. Hesse, Inverted hysteresis and giant exchange bias in $La_{0.7}Sr_{0.3}MnO_3$/$SrRuO_3$ superlattices, Appl. Phys. Lett. **97**, 052504 (2010).

[28] B. Böhm, L. Fallarino, D. Pohl, B. Rellinghaus, K. Nielsch, N. S. Kiselev, and O. Hellwig, Antiferromagnetic domain wall control via surface spin flop in fully tunable synthetic antiferromagnets with perpendicular magnetic anisotropy, Phys. Rev. B **100**, 140411(R) (2019).

[29] O. Hellwig, A. Berger, J. B. Kortright, and E. E. Fullerton, Domain structure and magnetization reversal of antiferromagnetically coupled perpendicular anisotropy films, J. Magn. Magn. Mater. **319**, 13 (2007).

[30] S. Emori, R. E. Maizel, G. T. Street, J. L. Jones, D. A. Arena, P. Shafer, and C. Klewe, Quantifying the orbital-to-spin moment ratio under dynamic excitation, Appl. Phys. Lett. **124**, 122404 (2024).

[31] N. S. Kiselev, I. E. Dragunov, U. K. Rößler, and A. N. Bogdanov, Exchange shift of stripe domains in antiferromagnetically coupled multilayers, Appl. Phys. Lett. **91**, 132507 (2007).

[32] S. Soltan, S. Macke, S. E. Ilse, T. Pennycook, Z. L. Zhang, G. Christiani, E. Benckiser, G. Schütz, and E. Goering, Ferromagnetic order controlled by the magnetic interface of $LaNiO_3$/$La_{2/3}Ca_{1/3}MnO_3$ superlattices, Sci. Rep. **13**, 3847 (2023).

[33] C. Piamonteze, M. Gibert, J. Heidler, J. Dreiser, S. Rusponi, H. Brune, J.-M. Triscone, F. Nolting, and U. Staub, Interfacial properties of $LaMnO_3$/$LaNiO_3$ superlattices grown along (001) and (111) orientations, Phys. Rev. B **92**, 014426 (2015).

[34] J. Schöpf (2024), doi:10.5281/zenodo.13443159.